metals

MDPI

Article

Effect of Friction Stir Welding and Tempering on the Microstructure and Strength of a Tempformed Low-Alloy Steel

Anastasiia S. Dolzhenko [1], Anna S. Lugovskaya [1], Sergey Malopheyev [1], Valeriy Dudko [1], Marina Tikhonova [1], Rustam Kaibyshev [2] and Andrey Belyakov [1,*]

[1] Laboratory of Mechanical Properties of Nanostructured Materials and Superalloys, Belgorod National Research University, Belgorod 308015, Russia; dolzhenko_a@bsu.edu.ru (A.S.D.); 1319927@bsu.edu.ru (A.S.L.); malofeev@bsu.edu.ru (S.M.); dudko@bsu.edu.ru (V.D.); tikhonova@bsu.edu.ru (M.T.)

[2] Moscow Timiryazev Agricultural Academy, Russian State Agrarian University, Moscow 127550, Russia; kajbyshev@rgau-msha.ru

* Correspondence: belyakov@bsu.edu.ru; Tel.: +7-472-258-5457

Abstract: The microstructure developed in a low-alloy steel during friction stir welding and post-weld tempering was studied. The quenched steel samples were subjected to tempering at 650 °C for 1 h, followed by warm rolling to a total strain of 1.5 at the same temperature. The processed steel samples were characterized by an ultrafine-grained microstructure of the lamellar type with a transverse grain size of 360 nm and exhibited an yield strength of about 1200 MPa and a total elongation of 13%. Then, the steel plates were joined by friction stir welding. The yield strength of the weld joint was about 1170 MPa, although the total elongation decreased to 1.5%. The martensite microstructure, with a high-angle grain boundary spacing of about 800 nm, was developed in the stir zone. This martensite in the stir zone originated from the ultrafine-grained prior austenite, resulting in an almost two-fold increase in hardness as compared to the base material. Tempering of the welded sample at 650 °C for 1 h resulted in a decrease in the hardness of the weld joint to the level of the base material. Nevertheless, the fracture of the welded and tempered sample occurred in the base material. The yield strength of the welded sample after tempering was 930 MPa, with a total elongation of 13%.

Keywords: high-strength low-alloy steel; tempforming; friction stir welding; strength and plasticity

Citation: Dolzhenko, A.S.; Lugovskaya, A.S.; Malopheyev, S.; Dudko, V.; Tikhonova, M.; Kaibyshev, R.; Belyakov, A. Effect of Friction Stir Welding and Tempering on the Microstructure and Strength of a Tempformed Low-Alloy Steel. *Metals* **2024**, *14*, 114. https://doi.org/10.3390/met14010114

Academic Editor: Masahiro Fukumoto

Received: 15 December 2023
Revised: 9 January 2024
Accepted: 15 January 2024
Published: 17 January 2024

1. Introduction

High-strength low-alloy steels are one of the most generally employed structural materials, offering a good price–property combination. A wide range of strength levels easily achievable using a relatively simple heat treatment, along with fair weldability, makes these steels very popular materials for various applications around the world [1,2]. A little drawback of the low-alloy steel processed in a high-strength state is the rather high temperature of the ductile-to-brittle transition, which may be just below room temperature [3–5]. This negative aspect somewhat limits the range of structural applications of high-strength low-alloy steels under low-temperature conditions.

A special thermo-mechanical treatment, tempforming, involving martensite tempering followed by large strain warm rolling, has been recently proposed to obtain high-strength carbon steels with exceptionally high impact toughness at low temperatures down to cryogenic conditions [6,7]. Such a tempforming treatment, including either bar rolling or plate rolling at tempering temperatures, was then successfully applied to various high-strength low-alloy steels, resulting in a unique strengthening effect, namely, increasing both tensile strength and impact toughness [8]. This beneficial combination of mechanical properties is attained owing to the ultrafine-grained microstructure evolved during warm rolling, which consists of highly elongated grains with homogeneously distributed finely dispersed oxide particles and a fiber texture of <001> along the normal direction (in the

case of plate rolling) or along the side direction (in bar rolling) [9,10]. The strengthening of the tempformed steels is provided by the high dislocation density associated with grain refinement and second-phase dispersion [10]. On the other hand, the high impact toughness is attributed to the delamination of the tempformed lamellar-type microstructure, which leads to zigzag branching of the main crack propagating across the impact specimen and increasing the absorbed energy [11].

The ultrafine-grained microstructure of lamellar-type is a principle factor responsible for the beneficial property combination of the steels processed by tempforming. On the other hand, such ultrafine-grained microstructure complicates the welding of tempformed steels because conventional welding techniques accompanied by partial melting of the base material may completely destroy the original valuable microstructure. This difficulty can be overcome by applying a promising solid-state welding method, i.e., friction stir welding (FSW) [12]. By now, FSW has been successfully used for various aluminum, magnesium, nickel, and copper alloys. FSW allows for obtaining a strength of the weld joint close to that of the base material using appropriate speeds for tool rotation and welding [12].

Recently, FSW has been applied to advanced high-strength steels, including a low-alloy steel processed by tempforming [13–17]. The developed microstructure in the stir zone consists of fine grains that resulted from martensitic transformation owing to heating over Ac_3 temperature during FSW, followed by rapid cooling behind the FSW tool [16,17]. Therefore, the FSW seam is characterized by an increased hardness as compared to the base material [14,17]. As a result, the fracture of the tensile specimen cut across the FSW joint occurs in the heat-affected zone, which is located close to the stir zone, leading to the strength of the FSW joint sample being just below the strength of the base material subjected to tempforming [17]. On the other hand, elongation of the FSW joint specimen does not exceed several percent.

Therefore, the thermal history should be controlled during FSW to enhance the joint properties of high-strength steels [14]. Alternatively, the plasticity of hardened steels can be improved using an appropriate tempering treatment. Equalizing the strength across the FSW joint should be expected during post-weld tempering. The uniform strength of the FSW joint should improve the deformation homogeneity, advancing the uniform elongation upon tensile testing. Thus, the aim of the present study is to investigate the effect of additional tempering on the microstructure and the mechanical properties of an FSW joint made of tempformed high-strength low-alloy steel.

2. Materials and Methods

A low-alloy steel with a chemical composition of 0.36% C, 0.4% Si, 0.56% Cr, 0.57% Mn, 0.54% Mo, 0.0067% P, 0.0034% S, and Fe—balance (all in mass%) was hot rolled at 1123 K, followed by water quenching. Then, the steel samples were subjected to a tempforming treatment. Namely, the steel samples were tempered for 1 h at 650 °C, followed by multiple rolling at the same temperature to a total strain of 1.5. The tempformed steel plates of 5 mm in thickness were joined by FSW using an AccuStir 1004 FSW machine with the weld seam parallel to the transverse direction (TD) of the rolled plates. A tool with a shoulder diameter of 11.26 mm and a semispherical pin of 2.4 mm in radius made of tungsten carbide was used with a rotation speed of 400 rpm and a travel speed of 50 mm/min (Figure 1). The present FSW tool is shown in Figure 2. Then, a part of the FSW joint sample was subjected to post-weld tempering at 650 °C for 1 h.

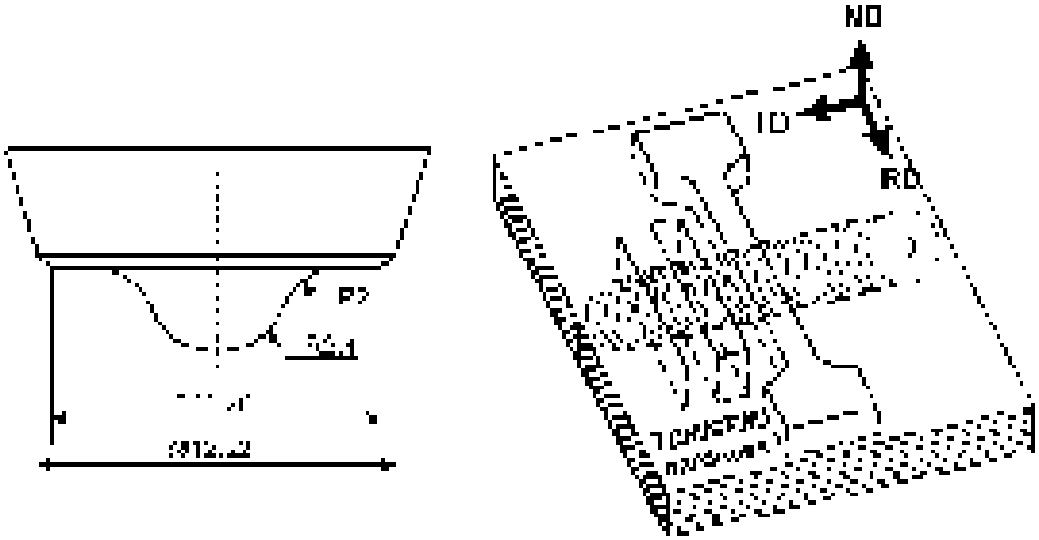

Figure 1. Drawing of the FSW tool and scheme of the FSW joint sample.

Figure 2. FSW tool before (**left**) and after (**right**) welding.

The microstructural observations of the FSW joint were carried out on the transverse section (TD plane) using a Quanta 600 FEG scanning electron microscope (SEM) equipped with an electron back-scattering diffraction (EBSD) pattern analyzer incorporating an orientation imaging microscopy (OIM) system with the TSL OIM software and a JEOL JEM-2100 transmission electron microscope (TEM). The microstructures after FSW and after post-weld tempering were studied in the center portion of the stir zone as well as in the base material. The SEM and TEM specimens were electro-polished using a 10% solution of perchloric acid in acetic acid at a voltage of 20 V. The OIM images were subjected to a cleanup procedure using the grain dilation technique, setting 3 points as the minimal grain size. The mean grain size was evaluated on the OIM images as the average distance between the high-angle grain boundaries with misorientations of $\theta \geq 15^{\circ}$. The dislocation density associated with low-angle sub-boundaries was calculated as follows [18]: $\rho_{OIM} = 1.5\ Sv\ \theta/b$, where Sv is the sub-boundary area per unit volume, θ is the sub-boundary misorientation, and b is the Burgers vector. The Sv value was calculated using the total length of subgrain boundaries with $2^{\circ} \leq \theta < 15^{\circ}$, as revealed by OIM. The precipitate particle size was measured on typical TEM images of the fine structure, counting at least 150 particles per data point. The dislocation density inside the grains/subgrains (ρ_{TEM}) was measured by counting individual dislocations on at least 4 typical TEM images. The misorientations of

the grain/subgrain boundaries observed by TEM were estimated using the Kikuchi lines obtained by a converged electron beam [19].

Vickers hardness was measured using a 402MVD Wolpert unit with a load of 3 N and a dwell time of 10 s. In order to clarify the hardness variation after FSW, a series of hardness measurements with a step of 0.5 mm were carried out along a line crossing the FSW joint. The tensile tests were carried out using an Instron 5882 testing machine at ambient temperature and a crosshead rate of 2 mm/min using two specimens with a gauge length of 35 mm and a cross section of 7×3 mm^2, with the tensile direction along the rolling direction (RD), i.e., crosswise the FSW seam. A digital image correlation technique was used to visualize the strain distribution by correlation of the successive images of a speckle pattern painted on the specimen surface using the Vic-3D correlation software [20].

3. Results

3.1. Hardness Distribution

The general view of the cross section of the as-welded joint is shown in Figure 3. The circle arc in Figure 3 represents the track left by the FSW tool. Thus, the two plates of the base material and the stir zone of the weld join are clearly visible in Figure 3. The used FSW geometry did not provide complete welding across the sample thickness. The lack of penetration is observed under the pin path in Figure 3. This drawback requires further elaboration using advanced FSW techniques, like bobbin tool FSW or self-supported FSW [21]. The present study is focused on the microstructure–property relationship for tempformed steel samples subjected to FSW. In order to reveal the strengthening/softening effect of FSW on the tempformed steel, the hardness was measured along the black line indicated in Figure 3.

Figure 3. Cross section of the FSW joint sample.

The hardness variation across the FSW joint is shown in Figure 4 for two conditions, i.e., the as-welded one (open symbols) and that followed by tempering (closed symbols). The base material subjected to tempforming exhibits a hardness of about 3500 MPa. FSW results in significant hardening of the tempformed steel. Hardness in the stir zone increases almost two-fold and reaches 7000 MPa. On the other hand, a small decrease in hardness to about 3000 MPa can be observed in the narrow region just between the stir zone and the base material. This portion can be considered a heat-affected zone analogously to conventional welding methods involving local melting of welded materials. The subsequent tempering equalizes the hardness across the FSW joint at a level of about 3000 MPa. It is worth noting that the heat-affected zone is characterized by a little lower hardness compared to the base material and the stir zone, even after tempering. The small drops in the hardness profile can be seen at 5 to 6 mm from the center of the welded joint.

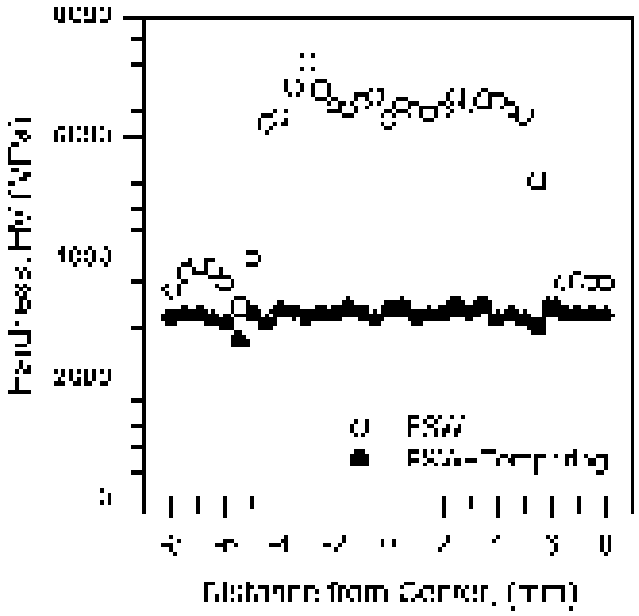

Figure 4. Hardness distribution across the FSW joint along the black line in Figure 3.

3.2. Microstructure Evolution

Microstructures evolved by tempforming at 650 °C have been described in detail elsewhere [10]. It can be briefly noted here that tempforming results in a lamellar-type microstructure consisting of elongated ultrafine grains with a transverse grain size of 360 nm and uniformly distributed dispersed carbide particles with an average size of 53 nm. The dislocation density is 3.3×10^{15} m^{-2}, including dislocations in the sub-boundaries and dislocations inside the grains/subgrains of the tempformed steel samples.

Typical microstructures evolved in the tempformed steel samples by FSW and subsequent tempering are shown in Figure 5. The stir zone is characterized by a lath martensite microstructure consisting of ultrafine crystallites (Figure 5a). The mean grain size in the stir zone is 850 nm. Evidently, the microstructure in the stir zone experienced austenite reversal, followed by martensitic transformation during FSW. Heating well above Ac_3 temperature, followed by rapid cooling resulting in a martensitic transformation, has been reported in other studies on the FSW of martensitic steels [16,22,23]. The density of dislocations arranged in low-angle sub-boundaries of the developed martensite in the stir zone is $\rho_{OIM} = 9 \times 10^{14}$ m^{-2}. Subsequent tempering at 650 °C for 1 h of the FSW joint sample results in the development of a tempered martensite microstructure in the stir zone (Figure 5b). The mean grain size of about 850 nm developed in the stir zone during FSW does not change remarkably upon subsequent tempering. On the other hand, the dislocation density in low-angle sub-boundaries slightly decreases to $\rho_{OIM} = 8 \times 10^{14}$ m^{-2}. The base material in the FSW joint subjected to post-weld tempering is characterized by a lamellar-type microstructure much similar to the original tempformed microstructure (Figure 5c). However, the additional post-weld tempering results in an increase in the transverse grain size of the base materials to 570 nm. It should be noted that the microstructure evolved in the base material consists of numerous low-angle sub-boundaries bearing a high dislocation density of $\rho_{OIM} = 1.3 \times 10^{15}$ m^{-2}.

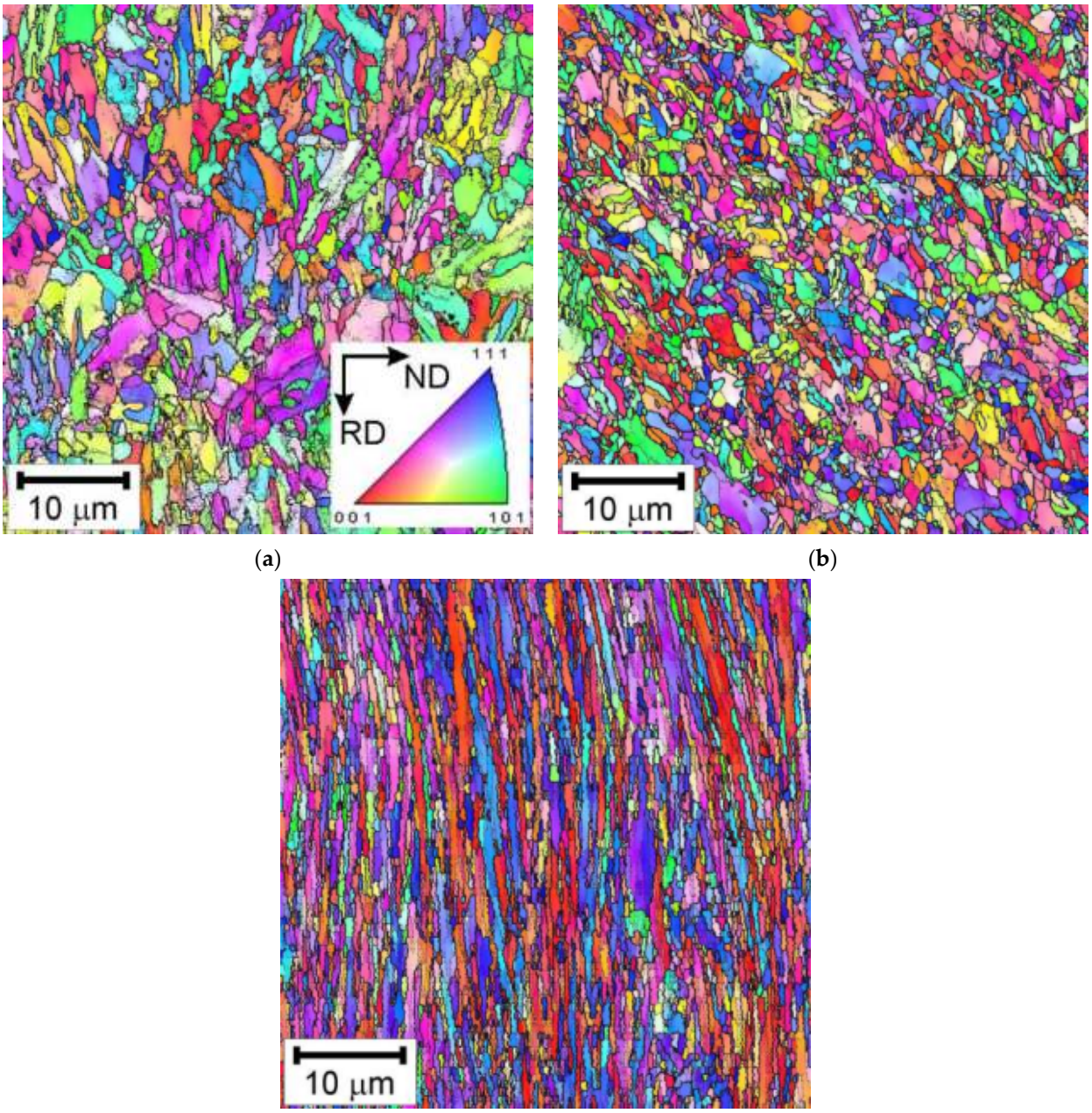

(**a**) (**b**)

(**c**)

Figure 5. Typical OIM microstructures in the stir zone after FSW (**a**), after FSW and tempering (**b**), and in the base material after FSW and tempering (**c**). Orientations are shown for the normal direction (ND).

The grain boundary misorientation distributions evolved in the stir zone of the FSW joint sample before and after post-weld tempering and in the base material after a post-weld treatment are shown in Figure 6. The misorientation distribution characters correspond to the microstructure evolution mechanisms operating at a previous treatment. The grain boundary misorientation distribution evolved on the stir zone corresponds to a martensite microstructure (Figure 6a). Thus, this misorientation distribution looks like a bimodal one with two peaks reflecting the large fractions of low-angle dislocation sub-boundaries and around 60° high-angle boundaries. The former results from numerous dislocation lath boundaries of the martensite structure, whereas the latter represents one of the frequent inter-variant misorientations between the martensite packets/blocks [24,25]. The subsequent tempering does not lead to any qualitative changes in the grain boundary

misorientation distribution in the stir zone (Figure 6b). The changes in the misorientation distribution upon tempering are of quantitative character. Namely, the fraction of low-angle sub-boundaries with misorientations of 2–4° decreases almost two-fold, leading to a little increase in the fractions of the high-angle boundaries. The microstructures evolved in the tempformed steel were affected by a large strain warm rolling. The grain boundary misorientation distributions developed during large strain deformation are commonly characterized by a small peak against low-angle sub-boundaries superimposed over a flat-type distribution with almost the same fractions of various high-angle misorientations [26]. In the case of uniaxial deformation, like rolling or drawing, an increase in the total strain may be accompanied by an increase in the fraction of the high-angle boundaries with misorientations close to 60° [27]. It is clearly seen in Figure 6c that the post-weld tempering does not affect the grain boundary misorientation distribution developed in the base material during tempforming. The corresponding misorientation distribution can be described as a smooth one with low and wide peaks for the low-angle sub-boundaries and high-angle grain boundaries.

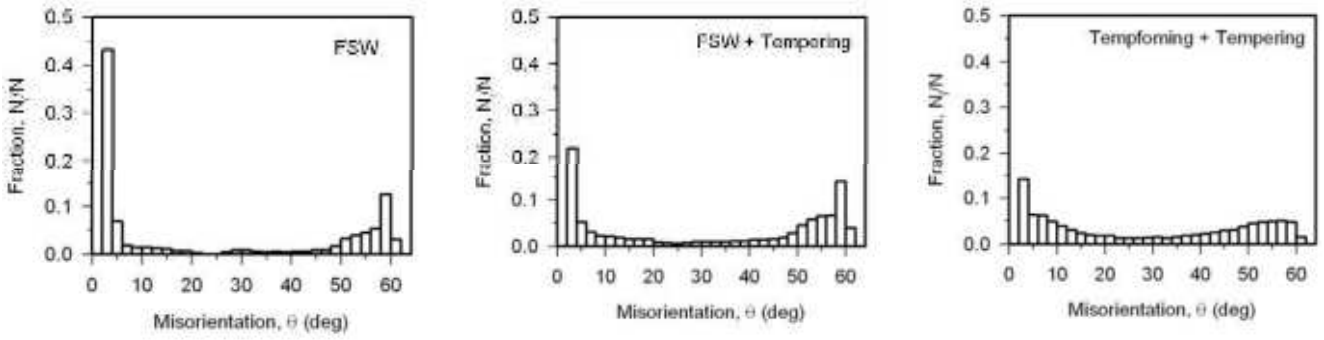

(**a**) (**b**) (**c**)

Figure 6. Grain boundary misorientation distributions in the stir zone after FSW (**a**), after FSW and tempering (**b**), and in the base material after FSW and tempering (**c**).

Typical TEM images of the fine structures evolved in the stir zone and the base material are represented in Figures 7–9. The lath martensite developed in the stir zone is characterized by a very high dislocation density of $\rho_{TEM} = 3 \times 10^{15}$ m^{-2} inside the laths (Figure 7). This value of the dislocation density exceeds that of $\rho_{OIM} = 9 \times 10^{14}$ m^{-2} associated with the low-angle sub-boundaries of the same FSW sample more than three times. Hence, the total dislocation density ($\rho = \rho_{OIM} + \rho_{TEM} = 3.9 \times 10^{15}$ m^{-2}) in the present FSW seam results mainly from the internal dislocations retained in the martensite laths. The post-weld tempering of the FSW joint leads to a significant decrease in the dislocation density in the stir zone (Figure 8). The density of the dislocations inside the tempered martensite laths/subgrains in the stir zone is $\rho_{TEM} = 8 \times 10^{14}$ m^{-2}, which is almost the same as the dislocation density related to the low-angle sub-boundaries. Besides the recovery of the dislocation substructure in the stir zone, tempering of the FSW joint provides the precipitation of finely dispersed $Cr_{23}C_6$-type carbide particles with an average size of 61 nm. The volume fraction of $Cr_{23}C_6$-type carbide in the present steel at 650 °C is 0.0669, as calculated by ThemoCalc [10]. The lowest dislocation density of $\rho_{TEM} = 3 \times 10^{14}$ m^{-2} inside the fine grains/subgrains among the studied portions of the FSW joint subjected to post-weld tempering is observed in the base material (Figure 9). In contrast to the stir zone, where the total dislocation density is mainly associated with the dislocations inside the laths/subgrains, the total dislocation density of $\rho = 1.6 \times 10^{15}$ m^{-2} in the base material after tempering is mainly controlled by the low-angle sub-boundaries. Additional tempering promotes particle coarsening in the base material. The average size of the dispersed particles in the base material increases to 77 nm during the post-weld treatment. The main microstructural parameters are listed in Table 1.

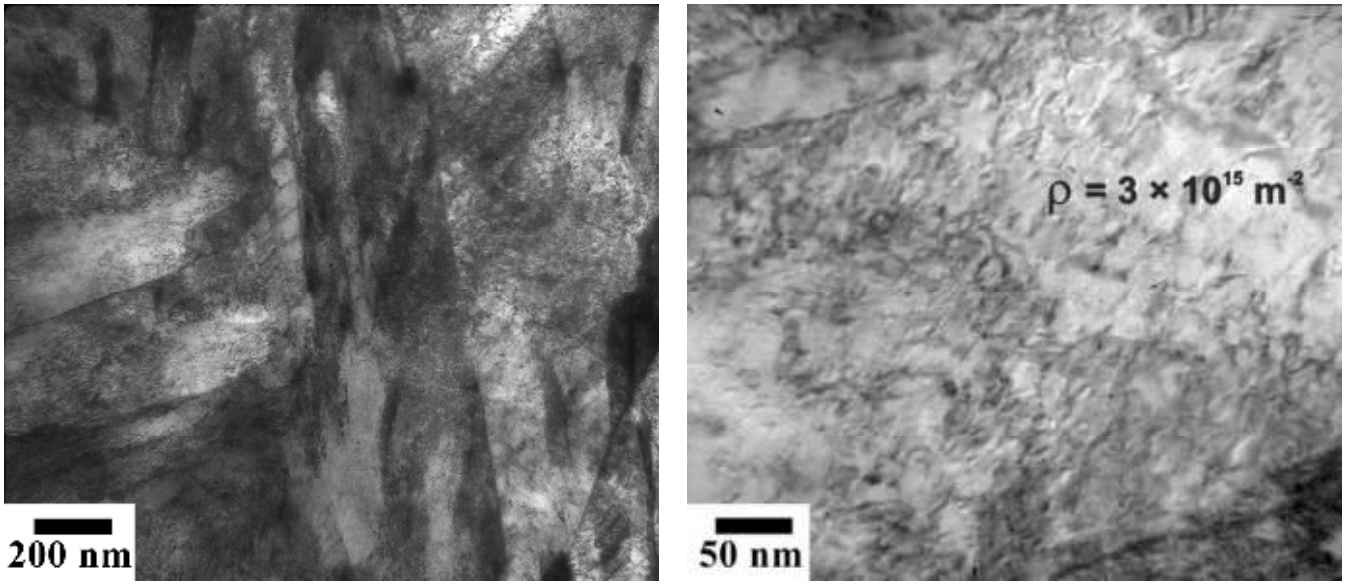

(**a**) (**b**)

Figure 7. Typical TEM image of the lath martensite (**a**) with high dislocation density of 3×10^{15} m^{-2} inside the laths (**b**) in the stir zone after FSW.

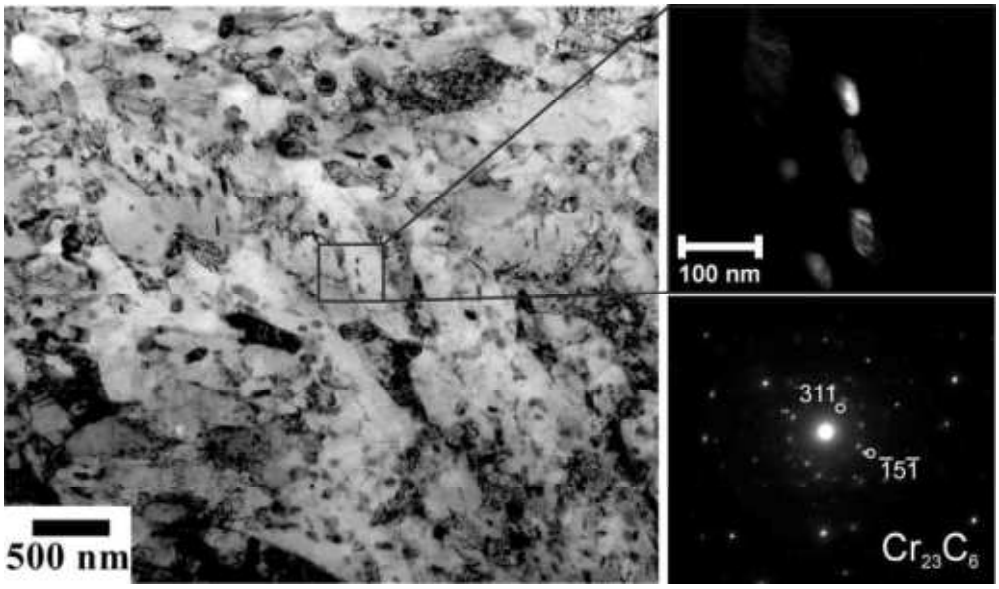

Figure 8. Typical TEM image of the tempered martensite in the stir zone after FSW and tempering.

Table 1. Some microstructural parameters, i.e., grain size (D), dislocation density (ρ), and dispersed particle size (d), of a high-strength low-alloy steel after tempforming and FSW followed by tempering.

Sample	D, nm	ρ_{OIM}, m^{-2}	ρ_{TEM}, m^{-2}	ρ, m^{-2}	d, nm
As-tempformed	360 ± 30	$(2.5 \pm 0.2) \times 10^{15}$	$(0.8 \pm 0.2) \times 10^{15}$	3.3×10^{15}	53 ± 8
FSW, stir zone	850 ± 80	$(0.9 \pm 0.1) \times 10^{15}$	$(3.0 \pm 0.6) \times 10^{15}$	3.9×10^{15}	-
FSW, stir zone, tempered	850 ± 80	$(0.8 \pm 0.1) \times 10^{15}$	$(0.8 \pm 0.2) \times 10^{15}$	1.6×10^{15}	61 ± 5
FSW, base material, tempered	570 ± 50	$(1.3 \pm 0.1) \times 10^{15}$	$(0.3 \pm 0.1) \times 10^{15}$	1.6×10^{15}	77 ± 8

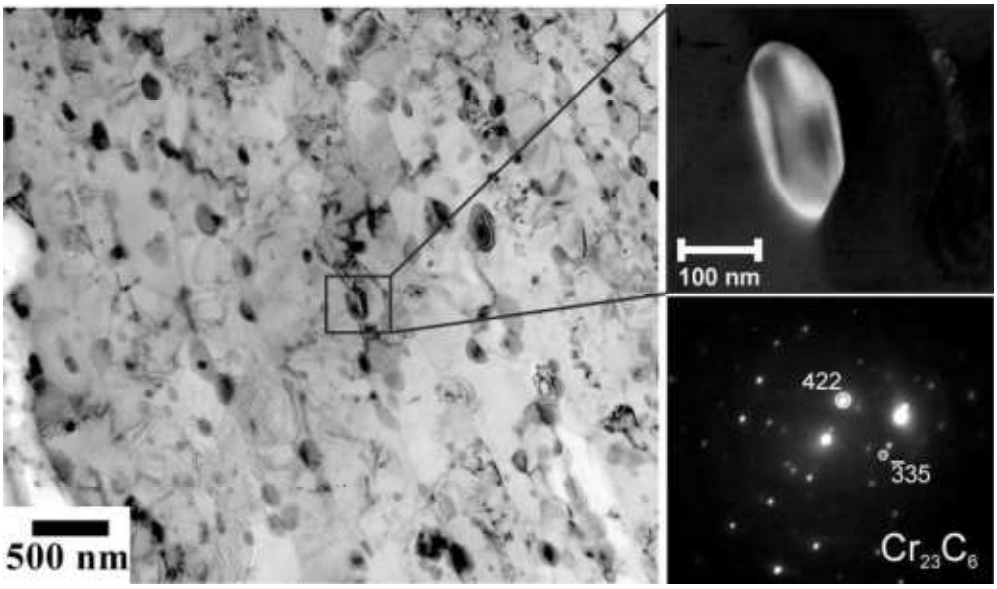

Figure 9. Typical TEM image of the base material of the FSW joint subjected to post-weld tempering.

3.3. Tensile Tests

Typical engineering stress–strain curves for the samples cut of the FSW joint and FSW joint subjected to post-weld tempering are shown in Figure 10, along with the stress–strain curve of the as-tempformed steel (the base material [10]) sample. The FSW joint sample is characterized by high strength, with an yield strength of $\sigma_{0.2}$ = 1170 MPa and an ultimate tensile strength of UTS = 1230 MPa. The strength of the FSW joint is almost the same as that of the base material, with $\sigma_{0.2}$ and UTS of about 1200 MPa. However, in contrast to the base material, which exhibits a total elongation of about 13%, the total elongation of the FSW joint sample is about 1.5%. The strain distribution along the tensile specimen made of the FSW joint is shown on the right side of Figure 10 for three points on the stress–strain curve, lettered by A, B, and C. It is clearly seen in the strain distribution images that the tensile deformation localizes in the base material quite close to the stir zone, i.e., the heat-affected zone. On the other hand, the stir zone remains almost non-deformed during the tensile test. Indeed, the stir zone is much harder than the base material (two times the difference in hardness in Figure 4). Thus, the rapid strain localization in the heat-affected zone is responsible for the small elongation of the as-processed FSW joint sample.

The post-weld tempering treatment remarkably improves the tensile plasticity of the FSW joint. Namely, the total elongation increases to about 13%, which is almost the same as that of the base material. However, an increase in plasticity is accompanied by a decrease in strength. The yield and ultimate tensile strength of the FSW joint decrease to 930 MPa after additional tempering. Generally, the stress–strain curve for the tempered FSW joint sample is very similar in appearance to that of the base-tempformed material. Following the discontinuous yielding, the flow stress remains at the same level until about 5% elongation, when necking occurs, followed by failure. The difference in the tensile behavior between the tempered FSW joint sample and the as-tempformed one is the tensile stress level. The tensile stresses of the FSW and tempered samples are lower by about 250 MPa than those of the original tempformed steel sample. In spite of the same hardness across the tempered FSW sample (Figure 4), the stir zone in the tensile specimen is characterized by a smaller deformation compared to the base material. The strain localization and subsequent fracture take place in the base material, as seen in the D to G images of the strain distribution visualization in Figure 10. Therefore, the increased plasticity of the FSW joint after the post-weld tempering treatment is associated with increased plasticity of the base material. It should be noted that the narrow soften regions in the heat-affected zone do not remarkably affect the tensile behavior of the FSW joint after tempering.

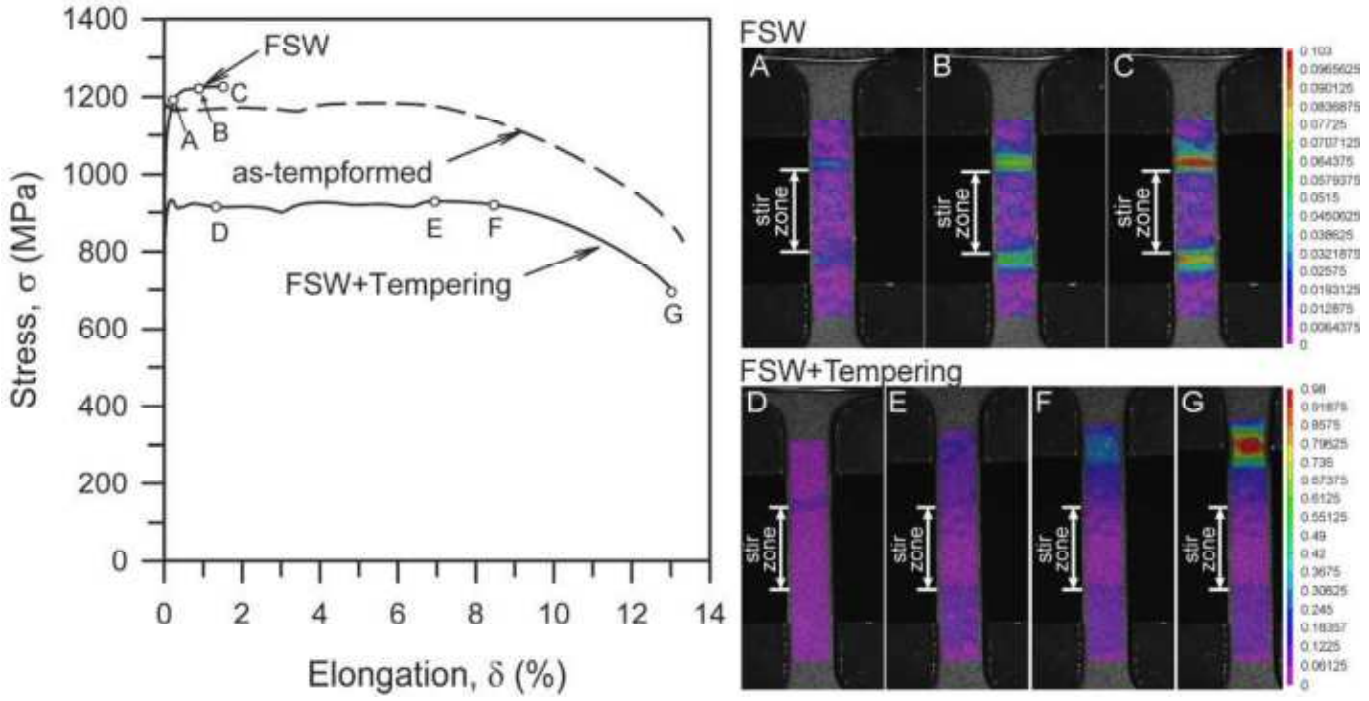

Figure 10. Engineering stress–strain curves and images of strain distribution at the indicated points during tensile tests of FSW joint samples after FSW and after FSW followed by tempering.

4. Discussion

The present results testify that FSW can be used to join high-strength low-alloy steels processed by tempforming, with the strength of the FSW joint comparable to the strength of the base material. Let us consider the strength–microstructure relationships in the obtained FSW joint sample. The strength of high-strength low-alloy steels is governed by their microstructure, which, in turn, depends on their evolutional mechanisms operating upon processing. The strengthening mechanisms deserving consideration for the present steel are dislocation strengthening ($\Delta\sigma_\rho$), grain size (or grain boundary) strengthening ($\Delta\sigma_D$), and dispersion strengthening ($\Delta\sigma_{Or}$), in addition to conventional lattice friction and solid solution strengthening [28,29]. The dislocation strengthening can be expressed by the following relationship [30]:

$$\Delta\sigma_\rho = \alpha G b \rho^{0.5}, \quad (1)$$

where α is a constant of about 0.9 [31] and G is the shear modulus of 81,000 MPa [32]. The grain size strengthening can be expressed by the second term of the Hall–Petch relationship as follows [33,34]:

$$\Delta\sigma_D = k_y D^{-0.5}, \quad (2)$$

where k_y and D are the grain boundary strengthening factors of about 0.24 MPa $m^{0.5}$ for low-carbon steel [35,36] and grain size, respectively. Assuming the Orowan mechanism for dislocation interactions with incoherent particles, the dispersion strengthening can be evaluated as follows [37]:

$$\Delta\sigma_{Or} = 0.45\ G b \lambda^{-1} \ln(d/b), \quad (3)$$

where λ is the edge-to-edge interparticle distance and d is the particle size.

The strengthening values calculated by Equations (1)–(3) for the as-tempformed, FSW, and FSW and tempered samples are shown in Table 2. The high strength after tempforming is attributed to the dislocation strengthening owing to the high dislocation density in numerous low-angle sub-boundaries. On the other hand, the relatively low dislocation density in the grain/subgrain interiors of the tempformed sample provides a rather large total elongation of the corresponding specimen. In contrast, FSW is accompanied by austenitization followed by rapid cooling of the stir zone, leading to martensitic transformation. The

high strength of the stir zone, hence, depends mainly on the high dislocation density inside the martensite laths. The post-weld tempering treatment decreases the dislocation density inside the martensite laths of the stir zone, decreasing the corresponding strengthening. It should be noted that the post-weld tempering treatment decreases the strengthening of the base material, i.e., the tempformed sample. Since tempforming consisted of tempering followed by large strain warm rolling, a remarkable recovery of the dislocation substructure accompanied by a little grain/subgrain coarsening should be expected upon subsequent annealing. It is interesting to note that the dislocation strengthening after post-weld tempering is roughly the same as that caused by both grain size and dispersed particles for the FSW seam and the base material. The same relationship between the different strengthening mechanisms has been reported for tempformed steels [10,38]. Takaki's group suggested that the strength increment of work-hardened steels can be expressed by a unique function of the dislocation density, which involves grain size and alloying effects [31,39].

Table 2. Yield strength ($\sigma_{0.2}$) and strengthening contributions from dislocation density ($\Delta\sigma_{\rho}$), grain size ($\Delta\sigma_{D}$), and dispersed particles ($\Delta\sigma_{Or}$) of a high-strength low-alloy steel after tempforming and FSW followed by tempering.

Sample	$\sigma_{0.2}$, MPa	$\Delta\sigma_{\rho}$, MPa	$\Delta\sigma_{D}$, MPa	$\Delta\sigma_{Or}$, MPa
As-tempformed	1180 ± 35	1050	400	495
FSW, stir zone	1170 ± 35	1140	260	-
FSW, stir zone, tempered	930 ± 20	730	260	455
FSW, base material, tempered	930 ± 20	730	320	380

The present results of the strengthening calculation (Table 2) indicate that the dislocation density remains high enough to control the yield strength even after the post-weld tempering treatment of the FSW joint sample. Therefore, FSW followed by post-weld tempering can be considered an advanced method for joining high-strength low-alloy steels processed by tempforming. The strength of tempformed steel depends on the processing conditions, namely, rolling temperature and total strain [8]. A decrease in tempforming temperature and/or an increase in strain promote both strength and impact toughness. On the other hand, the strength of the FSW joint seems to depend mainly on the alloying extent of high-strength steels [15]. Steels with higher strength look more susceptible to hardening by FSW. Nevertheless, the final strength of the FSW joint of the tempformed steel subjected to a post-weld treatment is governed by the temperature/duration of the post-weld tempering. Thus, the post-weld tempering treatment allows for a wide strength range in the FSW joints made of high-strength tempformed steels. Since the strength of the FSW joint after post-weld tempering is controlled by dislocation density, the regularities of recovery can be utilized to predict the annealing softening and obtainable strength level in the processed steels, although the recovery development in tempformed steels deserves further investigation.

5. Conclusions

The microstructure and the mechanical properties of a high-strength low-alloy steel processed by tempforming, i.e., tempering and large strain warm rolling at 650 °C, and then subjected to friction stir welding (FSW) and a post-weld tempering treatment were studied. The main results can be summarized as follows:

1. The stir zone of the FSW joint sample is characterized by a lath martensite microstructure due to heating up to the austenite region and rapid cooling after the FSW. Owing to the high dislocation density inside the martensite laths, the hardness of the stir zone increases two-fold, reaching 7000 MPa. The yield strength of the FSW joint sample was 1170 MPa, which is comparable with that of about 1200 MPa of the base-tempformed material. The strain localization takes place in the heat-affected zone close to the stir

zone upon tensile testing of the FSW joint sample, leading to a small total elongation of about 1.5%.

2. Post-weld tempering at 650 °C for 1 h results in a decrease in the hardness of the weld joint to the level of the base material of about 3000 MPa. However, the strain localization followed by fracture upon tensile testing of the welded and tempered sample occurs in the base material. The yield strength of the FSW joint sample after tempering was 930 MPa, with a total elongation of 13%. This increase in elongation is attributed to further tempering and improving the plasticity of the base material. The yield strength is controlled by the dislocation density, which provides strengthening similar to that from grain size and dispersed particles.
3. FSW, followed by a post-weld tempering treatment, can be used to join high-strength low-alloy steels with an ultrafine-grained microstructure produced by tempforming.

Author Contributions: Conceptualization, A.B.; methodology, S.M.; validation, V.D.; formal analysis, M.T.; investigation, A.S.D., A.S.L. and S.M.; resources, R.K.; writing—original draft preparation, A.S.D., A.S.L. and S.M.; writing—review and editing, A.B., M.T., R.K. and V.D.; visualization, V.D.; supervision, R.K.; project administration, M.T.; funding acquisition, R.K. All authors have read and agreed to the published version of the manuscript.

Funding: This research was funded by the Russian Science Foundation (agreement number: 20-19-00497-P).

Data Availability Statement: The data presented in this study are available on request from the corresponding author.

Acknowledgments: The work was carried out using the equipment of the Joint Research Center, Technology and Materials, Belgorod National Research University.

Conflicts of Interest: The authors declare no conflicts of interest.

References

1. Goodwin, F.; Guruswamy, S.; Kainer, K.U.; Kammer, C.; Knabl, W.; Leichtfried, G.; Schlamp, G.; Stickler, R.; Warlimont, H. Metals. In *Springer Handbook of Condensed Matter and Materials Data*; Martienssen, W., Warlimont, H., Eds.; Springer: Berlin, Germany, 2005; pp. 161–430.
2. Krauss, G. *Steels: Processing Structure and Performance*; ASM International: Phoenix, AZ, USA, 2015; 681p.
3. Faucher, B.; Dogan, B. Evaluation of the fracture toughness of hot-rolled low-alloy Ti-V plate steel. *Metall. Trans. A* **1988**, *19*, 505–516. [CrossRef]
4. Tomita, Y. Low temperature mechanical properties of quenched and tempered 04C–Ni–Cr–Mo steel after controlled rolling. *Mater. Sci. Technol.* **1988**, *4*, 613–620. [CrossRef]
5. Tomita, Y. Low-temperature improvement of mechanical properties of AISI 4340 steel through high-temperature thermomechanical treatment. *Metall. Trans. A* **1991**, *22*, 1093–1102. [CrossRef]
6. Kimura, Y.; Inoue, T.; Yin, F.; Sitdikov, O.; Tsuzaki, K. Toughening of a 1500 MPa class steel through formation of an ultrafine fibrous grain structure. *Scripta Mater.* **2007**, *57*, 465–468. [CrossRef]
7. Kimura, Y.; Inoue, T.; Yin, F.; Tsuzaki, K. Inverse temperature dependence of toughness in an ultrafine grain-structure steel. *Science* **2008**, *320*, 1057–1060. [CrossRef] [PubMed]
8. Dolzhenko, A.; Kaibyshev, R.; Belyakov, A. Tempforming as an advanced processing method for carbon steels. *Metals* **2020**, *10*, 1566. [CrossRef]
9. Inoue, T.; Qiu, H.; Ueji, R.; Kimura, Y. Ductile-to-brittle transition and brittle fracture stress of ultrafine-grained low-carbon steel. *Materials* **2021**, *14*, 1634. [CrossRef]
10. Dolzhenko, A.; Kaibyshev, R.; Belyakov, A. Tempforming Strengthening of a Low-Alloy Steel. *Materials* **2022**, *15*, 5241. [CrossRef]
11. Kimura, Y.; Inoue, T. Influence of annealing on delamination toughening of Mo-bearing medium-carbon steel with ultrafine elongated grain structure processed by warm tempforming. *ISIJ Int.* **2022**, *62*, 402–404. [CrossRef]
12. Al-Sabur, R. Tensile strength prediction of aluminium alloys welded by FSW using response surface methodology—Comparative review. *Mater. Today Proc.* **2021**, *45*, 4504–4510. [CrossRef]
13. Santella, M.; Hovanski, Y.; Pan, T.-Y. Friction stir spot welding (FSSW) of advanced high strength steel (AHSS). *SAE Int. J. Mater. Manuf.* **2012**, *5*, 382–387. [CrossRef]
14. Lee, H.; Kim, C.; Song, J.H. An evaluation of global and local tensile properties of friction-stir welded DP980 dual-phase steel joints using a digital image correlation method. *Materials* **2015**, *8*, 8424–8436. [CrossRef]

15. You, H.; Kang, M.; Yi, S.; Hyun, S.; Kim, C. Comprehensive Analysis of the Microstructure and Mechanical Properties of Friction-Stir-Welded Low-Carbon High-Strength Steels with Tensile Strengths Ranging from 590 MPa to 1.5 GPa. *Appl. Sci.* **2021**, *11*, 5728. [CrossRef]
16. Abhilash, V.; Lakshminarayanan, A.K. Friction stir lap joining techniques effects on microstructure and tensile properties of high strength automotive steel top hat sections. *Mater. Res. Express* **2023**, *10*, 026505. [CrossRef]
17. Dolzhenko, A.; Lugovskaya, A.; Belyakov, A. Failure of friction stir welded joint of a tempformed high-strength low-alloy steel. In *Proceedings of the 16th Sino-Russia Symposium on Advanced Materials and Technologies*; The Nonferrous Metals Society of China: Beijing, China, 2023; pp. 240–244.
18. Hughes, D.A.; Hansen, N. Microstructure and strength of nickel at large strains. *Acta Mater.* **2000**, *48*, 2985–3004. [CrossRef]
19. Williams, D.B.; Carter, C.B. *Transmission Electron Microscopy*; Plenum Press: New York, NY, USA, 1996; pp. 289–318.
20. The VIC-3D System. Available online: https://www.correlatedsolutions.com/vic-3d/ (accessed on 15 December 2023).
21. Meng, X.; Huang, Y.; Cao, J.; Shen, J.; Dos Santos, J.F. Recent progress on control strategies for inherent issues in friction stir welding. *Prog. Mater. Sci.* **2021**, *115*, 100706. [CrossRef]
22. Ohashi, R.; Fujimoto, M.; Mironov, S.; Sato, Y.S.; Kokawa, H. Microstructural characterization of high-strength steel lap joint produced by friction spot joining. *Metall. Mater. Trans. A* **2009**, *40A*, 2033–2035. [CrossRef]
23. Hua, P.; Mironov, S.; Sato, Y.S.; Kokawa, H.; Park, S.H.C.; Hirano, S. Crystallography of martensite in friction-stir-welded 12 Cr heat-resistant steel. *Metall. Mater. Trans. A* **2019**, *50A*, 3158–3163. [CrossRef]
24. Kitahara, H.; Ueji, R.; Ueda, M.; Tsuji, N.; Minamino, Y. Crystallographic analysis of plate martensite in Fe–28.5at.% Ni by FE-SEM/EBSD. *Mater. Charact.* **2005**, *54*, 378–386. [CrossRef]
25. Kitahara, H.; Ueji, R.; Tsuji, N.; Minamino, Y. Crystallographic features of lath martensite in low-carbon steel. *Acta Mater.* **2006**, *54*, 1279–1288. [CrossRef]
26. Dolzhenko, A.; Tikhonova, M.; Kaibyshev, R.; Belyakov, A. Microstructures and Mechanical Properties of Steels and Alloys Subjected to Large-Strain Cold-to-Warm Deformation. *Metals* **2022**, *12*, 454. [CrossRef]
27. Belyakov, A.; Kimura, Y.; Adachi, Y.; Tsuzaki, K. Microstructure Evolution in Ferritic Stainless Steels during Large Strain Deformation. *Mater. Trans.* **2004**, *45*, 2812–2821. [CrossRef]
28. De Ardo, A.J.; Hua, M.J.; Cho, K.G.; Garcia, C.I. On strength of micro alloyed steels: An interpretive review. *Mater. Sci. Technol.* **2009**, *25*, 1074–1082. [CrossRef]
29. Xiong, Z.; Timokhina, I.; Pereloma, E. Clustering, nano-scale precipitation and strengthening of steels. *Prog. Mater. Sci.* **2021**, *118*, 100764. [CrossRef]
30. Mecking, H.; Kocks, U. Kinetics of flow and strain-hardening. *Acta Metall.* **1981**, *29*, 1865–1875. [CrossRef]
31. Tanaka, Y.; Takaki, S.; Tsuchiyama, T.; Uemori, R. Effect of grain size on the yield stress of cold worked iron. *ISIJ Int.* **2018**, *58*, 1927–1933. [CrossRef]
32. Frost, H.; Ashby, M. *Deformation Mechanism Maps*; Pergamon Press: Oxford, UK, 1982; p. 166.
33. Hall, E.O. The deformation and ageing of mild steel: III Discussion of results. *Proc. Phys. Soc. Sect. B* **1951**, *64*, 747–753. [CrossRef]
34. Petch, N.J. The cleavage strength of polycrystals. *J. Iron Steel Inst.* **1953**, *174*, 25–28.
35. Lesuer, D.R.; Syn, C.K.; Sherby, O.D. Influence of Iron Oxide Particles on the Strength of Ball-Milled Iron. *Mater. Trans.* **2006**, *47*, 1508–1517. [CrossRef]
36. Belyakov, A.; Tsuzaki, K.; Kimura, Y.; Mishima, Y. Tensile behaviour of submicrocrystalline ferritic steel processed by large-strain deformation. *Philos. Mag. Lett.* **2009**, *89*, 201–212. [CrossRef]
37. Harrell, T.J.; Topping, T.D.; Wen, H.; Hu, T.; Schoenung, J.M.; Lavernia, E.J. Microstructure and strengthening mechanisms in an ultrafine grained Al-Mg-Sc alloy produced by powder metallurgy. *Metall. Mater. Trans. A* **2014**, *45A*, 6329–6343. [CrossRef]
38. Dolzhenko, A.; Pydrin, A.; Gaidar, S.; Kaibyshev, R.; Belyakov, A. Microstructure and Strengthening Mechanisms in an HSLA Steel Subjected to Tempforming. *Metals* **2022**, *12*, 48. [CrossRef]
39. Takaki, S. Yielding behavior of polycrystalline ferritic steel. In *THERMEC'2021 Book of Abstracts, Proceedings of the International Conference on Processing & Manufacturing of Advanced Materials, Online, 1–5 June 2021*; Graz University of Technology: Graz, Austria, 2021; pp. 33–34.